1-D Dynamic Modeling of SOFC with Analytical Solution for Reacting Gas-Flow Problem

Yutong Qi, Biao Huang, and Jingli Luo
Dept. of Chemical and Materials Engineering, University of Alberta, Edmonton, AB, Canada, T6G 2G6

DOI 10.1002/aic.11433
Published online April 21, 2008 in Wiley InterScience (www.interscience.wiley.com).

A first principle one-dimensional (1-D) dynamic model for tubular solid oxide fuel cell (SOFC) is developed. To convert the distributed model into a control relevant nonlinear state space model, an approximate analytical solution for reacting gas-flow problem is proposed, and applied to the 1-D SOFC dynamic model. Compared to numerical solutions, the proposed solution can significantly reduce requirements in computation, and thus, facilitate dynamic simulations and control applications. Distributed dynamic relations between current density and electromotive force (EMF) are investigated. Diffusion, inherent impedance, primary flow, heat transfer, and internal reforming/shifting reaction are considered simultaneously. Dynamic responses of the interested variables when external current, fuel and air inlet streams are perturbed by step changes are investigated through simulations. © 2008 American Institute of Chemical Engineers *AIChE J,* 54: 1537–1553, 2008

Keywords: SOFC, dynamic model, distribute model, analytical solution, reacting gas flow

Introduction

With recent significant progress of SOFC prototype stacks, dynamic operation and control problems become increasingly important and, as a result, dynamic properties of SOFC stack need to be modeled and investigated. Advanced SOFC system configurations also need better understanding of SOFC dynamic characteristics to ensure system stability and operatability.

Dynamic modeling of SOFC originated from the lumped parameter assumptions.[1–5] Lumped models are simple enough in control relevant application, but may lead significant errors in presenting SOFC dynamics. For more accurate descriptions, distributed models were usually adopted.[6–9] Although some previously developed distributed model were built in the dynamic form, dynamic properties of SOFC have not been their focus.[7–9]

To build a suitable model that is accurate enough and useful for dynamic simulation and control, our previous work started by examining the dynamics induced by diffusion and inherent impedance.[10] Then in a finite volume of SOFC, we investigated and modeled dynamic effects from surrounded transport processes to the cell, and investigated the local dynamic properties through simulation.[11] Effects, such as radiation and enthalpy change led by mass exchange, etc. that was neglected before were also carefully considered and modeled.

In this article, we will extend our previous dynamic model from the finite volume to a complete tubular SOFC, considering dynamics distributions, such as current density, temperature, and mole fractions, etc., along the flow direction. The resultant 1-D dynamic model consists of a set of partial differential equations (PDEs) dependent on both time and axial position.

However, a complex 1-D dynamic model described by a set of PDEs is not suitable for general control applications.

Correspondence concerning this article should be addressed to B. Huang at biao.huang@ualberta.ca.

In a typical online control application, PDEs may need to be solved in every control interval. The distributed dynamic model developed may have heavy computation demands, and may not be suitable for online applications. In addition, the PDE form of the model creates more complexity in control design. The common practice to convert PDEs to ODEs is through numerical discretization. However, this will result in a very large set of ODEs. For example, numerical simulation of 1-D model developed by Iora et al., needs to solve 12,500 nonlinear equations simultaneously.[9]

Instead of relying on numerical solutions, we will consider a novel approach to solving the 1-D problem with considerably less requirements in computations as introduced next.

An 1-D dynamic model of a physical system is usually shown as

$$\begin{aligned}\frac{\partial v_1}{\partial t} &= -\frac{\partial h_1(\boldsymbol{v})}{\partial z} + f_1(\boldsymbol{v})\\ \frac{\partial v_2}{\partial t} &= -\frac{\partial h_2(\boldsymbol{v})}{\partial z} + f_2(\boldsymbol{v})\\ &\vdots\\ \frac{\partial v_n}{\partial t} &= \frac{\partial h_n(\boldsymbol{v})}{\partial z} + f_n(\boldsymbol{v})\end{aligned}$$

Obviously, the analytical solution of the above PEDs is most desirable for the purpose of control applications or even for dynamic simulations. However, it is very difficult, if not impossible, to solve the nonlinear nonhomogeneous PDE array explicitly. Instead, we will find an approximated analytical solution, and then convert the 1-D model into the control relevant ODE form of

$$\begin{aligned}\frac{dv_1}{dt} &= g_1(\boldsymbol{v}, z)\\ \frac{dv_2}{dt} &= g_2(\boldsymbol{v}, z)\\ &\vdots\\ \frac{dv_n}{dt} &= g_n(\boldsymbol{v}, z)\end{aligned} \tag{1}$$

where v_i represents physical variables, $\boldsymbol{v} = [v_1\ v_2\ \cdots\ v_n]'$, and z is the location along the flow direction.

This solution is attractive in the sense that simple substitution of position z into the model results in dynamic description at corresponding point. It does not need to integrate all PDEs all the way from the entry to exit in order to get the dynamics at point z; thus, the proposed strategy can significantly reduce computation efforts. These ordinary differential equations (ODEs) form a nonlinear statespace model (SSM), as function of z.

An approximated analytical solution for general 1-D reacting gas-flow problem is derived in this article. The result is then applied to the fuel and air flow in the SOFC stack and forms a semianalytical 1-D dynamic nonlinear state-space model. By means of dynamic simulation, distributed dynamic properties of SOFC are investigated through the step responses of each interested variables.

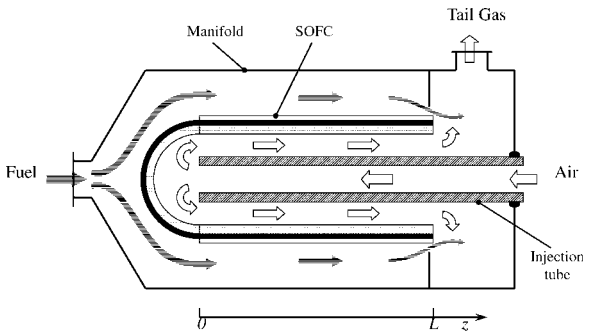

Figure 1. Tubular SOFC stack design.

1-D Dynamic Modeling of SOFC

Brief introduction to tubular SOFC

The tubular SOFC stack consists of hundreds of cell composites. Each composite consists of two tubes, SOFC cell and alumina air injection tube. The cell is an air-electrode-support (AES) tube, onto which the electrolyte is deposited, followed by the anode in the outer surface. Fuel gas is injected from the close end of composites, and flows over anode surface through channels formed by composites. Preheated air is injected from the injection tube to the bottom of the cell, then turning around and flowing over the cathode surface through the gap between the cell and the injection tube, as shown in Figure 1.

Reactants diffuse away from primary flows, pass through porous electrodes, and reach reaction sites, where they participate in the electrochemical reaction and produce current. The electromotive force (EMF) is established between the anode and the cathode reaction sites, as shown in Figure 2.

Electricity

Voltage Output. The electromotive force (EMF) in the SOFC is established through electrochemical reactions at triple-phase boundaries(*tpb*):

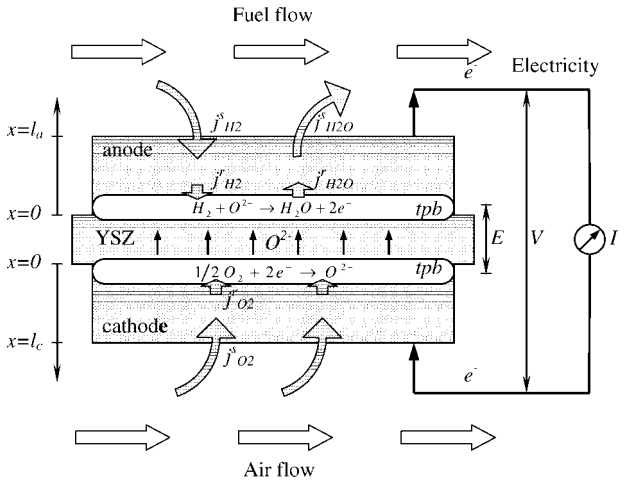

Figure 2. Secondary flows of reactant and electrochemical reactions.

$$H_2 + O^{2-} \rightarrow H_2O + 2e^-$$
$$\frac{1}{2}O_2 + 2e^- \rightarrow O^{2-}$$

or

$$CO + O^{2-} \rightarrow CO_2 + 2e^-$$
$$\frac{1}{2}O_2 + 2e^- \rightarrow O^{2-}$$

Because how CO and H_2 compete the reaction in the *tpb* is not clear in the following modeling process, CO is assumed not to participate in the electrochemical reaction.

The EMF is affected by temperature T and reactant partial pressures in the immediate vicinity of triple phase boundary (*tpb*) p^{tpb}, and reduced by the activation loss η_{act}[10]

$$E = E^0 + \frac{RT}{2F}\ln\left(\frac{p_{H_2}^{\text{tpb}} p_{O_2}^{\text{tpb}\frac{1}{2}}}{p_{H_2O}^{\text{tpb}}}\right) - \eta_{\text{act}} \tag{2}$$

Because we assume that no axial diffusion occurs in the cell, a local EMF is, therefore, independent of the EMF of the neighboring sections, and the distribution and dynamics of the EMF is, thus, determined by distributions of factors discussed earlier.

Due to the existence of inherent resistance and double layer capacitance, EMF is also dynamically deducted by the voltage drop on the intrinsic impedance of the SOFC. The effect was emulated by an equivalent circuit as proposed in Qi et al.[10] In this equivalence, the ionic resistance of the electrolyte and charge transfer resistances of the electrolyte-electrode interfaces are concluded by an single resistance R_{ct}. The resistances lies between the two electrodes, which form a capacitor C_{ct}. The pure Ohmic resistance of the two electrodes is represented by R_{o}. The dynamic behavior of the local voltage is then modeled through the equivalent circuit as

$$\begin{aligned} \dot{V}_{\text{ct}} &= \frac{1}{\rho_{R_{\text{ct}}}\rho_{C_{\text{ct}}}}E - \frac{1}{\rho_{R_{\text{ct}}}\rho_{C_{\text{ct}}}}V_{\text{ct}} - \frac{1}{\rho_{C_{\text{ct}}}}i \\ V_{\text{out}} &= V_{\text{ct}} - \rho_{R_{\text{o}}} i \end{aligned} \tag{3}$$

where i is the local current density, $\rho_{R\text{ct}}$ the specific resistance of R_{ct}, $\rho_{R\text{o}}$ the specific resistance of R_{o}, and $\rho_{C\text{ct}}$ the specific capacitance.

Current Density. Current density distribution is determined by the total current demand I and the distribution of EMF. Their relations can also be determined through the equivalent circuit approach.

Due to the large electrical conductivity of the interconnector beam, the voltage output V_{out} measured on the connector beam can be assumed uniform, and the equivalent circuit of the whole tube can be seen as a combination of N equivalent circuits of N sections,[10] as shown in Figure 3.

For this equivalent circuit, we have the following relations

$$\begin{aligned} V_{\text{ct},1} - R_{\text{o},1}I_1 &= V_{\text{ct},2} - R_{\text{o},2}I_2 \\ V_{\text{ct},2} - R_{\text{o},2}I_2 &= V_{\text{ct},3} - R_{\text{o},3}I_3 \\ &\vdots \\ V_{\text{ct,N}-1} - R_{\text{o,N}-1}I_{\text{N}-1} &= V_{\text{ct,N}} - R_{\text{o,N}}I_N \end{aligned} \tag{4}$$

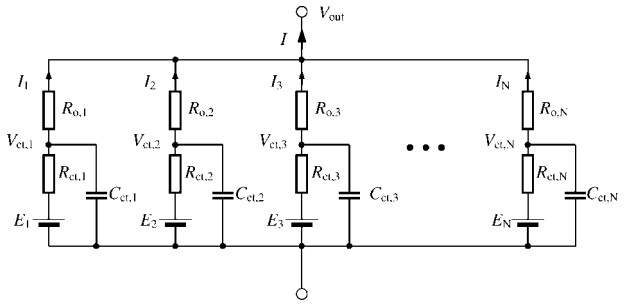

Figure 3. Equivalent circuit of SOFC tube.

and

$$I = I_1 + I_2 + \cdots + I_{\text{N}}$$

Totally N equations exist for the N unknown subcurrents I_i; I_i can then be solved from the equations.

The solutions of I_{i} are functions of I, $R_{\text{o},i}$ and $V_{\text{ct},i}$. Assuming that $R_{\text{o},i}$'s are the same, and $N \rightarrow \infty$, I_i then converge to the local current, and can be expressed as local current density

$$i = \frac{V_{\text{ct}} - \bar{V}_{\text{ct}}}{\rho_{\text{R}_{\text{o}}}} + \frac{I}{2\pi r_3 L} \tag{5}$$

where $\bar{V}_{\text{ct}}$ is the average potential of the whole tube, and L the length of the tube.

Diffusion

Reactants must be transported from primary flows to reaction sites to participate in the electrochemical reaction, as shown in Figure 2. Depending on the total effective diffusion coefficient and effective diffusion thickness, these processes was modeled dynamically by Qi et al.[10]

$$\begin{aligned} \ddot{j}_{H_2}^s &= -h_1 j_{H_2}^s - h_2 \dot{j}_{H_2}^s + h_1 \frac{1}{2F}\cdot i + h_3 \dot{C}_{H_2}^{\text{b}} \\ \ddot{j}_{O_2}^s &= -o_1 j_{O_2}^s - o_2 \dot{j}_{O_2}^s + o_1 \frac{1}{4F}\cdot i + o_3 \dot{C}_{O_2}^{\text{b}} \\ \ddot{j}_{H_2O}^s &= -w_1 j_{H_2O}^s - w_2 \dot{j}_{H_2O}^s - w_1 \frac{1}{2F}\cdot i + w_3 \dot{C}_{H_2O}^{\text{b}} \end{aligned} \tag{6}$$

and

$$\begin{aligned} \ddot{p}_{H_2}^{tpb} &= -h_1 p_{H_2}^{tpb} - h_2 \dot{p}_{H_2}^{tpb} - h_4 \frac{RT_{\text{cell}}}{2F}\cdot i - \frac{4}{l_{\text{a}}}\frac{RT_{\text{cell}}}{2F}\cdot \dot{i} + h_1 p_{H_2}^{b} \\ \ddot{p}_{O_2}^{tpb} &= -o_1 p_{O_2}^{tpb} - o_2 \dot{p}_{O_2}^{tpb} - o_4 \frac{RT_{\text{cell}}}{4F}\cdot i - \frac{4}{l_{\text{c}}}\frac{RT_{\text{cell}}}{4F}\cdot \dot{i} + o_1 p_{O_2}^{b} \\ \ddot{p}_{H_2O}^{tpb} &= -w_1 p_{H_2O}^{tpb} - w_2 \dot{p}_{H_2O}^{tpb} + w_4 \frac{RT_{\text{cell}}}{2F}\cdot i + \frac{4}{l_{\text{a}}}\frac{RT_{\text{cell}}}{2F}\cdot \dot{i} + w_1 p_{H_2O}^{b} \end{aligned} \tag{7}$$

where l_{a} and l_{c} are anode and cathode side diffusion layer thickness respectively; coefficients $h_{1\sim4}$, $o_{1\sim4}$ and $w_{1\sim4}$ are functions of diffusion coefficients and diffusion thicknesses. The local current density i determines the local reactant consumption rates: $i = 2Fj_{H_2}^r = -2Fj_{H_2O}^r = 4Fj_{O_2}^r$.

Solid-phase temperature

Cell Temperature. Reactants diffuse into the solid-phase cell, and produce electrical energy through the electrochemical reactions. The energy conversions affect the temperature of the cell, and consequently heat exchanges with the surrounding flow bodies, due to temperature differences, through convection and radiation. Because the endothermal reforming reaction takes place in the surface of anode, it also affects the cell temperature significantly.

The conductivity and the cross-section area of solid cell are relatively small; the heat flow due to conduction along the axial direction within the cell is, therefore, small, compared to that along the radius direction. Consequently, dynamic effects due to the conduction along the axial direction can be neglected.[11] Assuming that the reforming reaction occurs at the surface of the electrode, the energy balance for a small slice of cell is

$$\frac{dE_{\text{cell}}}{dt} = [(J^{\text{i}}_{\text{H}_2} - J^{\text{e}}_{\text{H}_2})H_{\text{H}_2} + (J^{\text{i}}_{\text{H}_2\text{O}} - J^{\text{e}}_{\text{H}_2\text{O}})H_{\text{H}_2\text{O}} + J^{\text{i}}_{\text{CH}_4}H_{\text{CH}_4} - J^{\text{e}}_{\text{CO}}H_{\text{CO}}] + J^{\text{s}}_{\text{O}_2}H_{\text{O}_2} - E_{\text{e}} - q_{\text{conv}} - q_{\text{rad}} \quad (8)$$

where J^{i} represents H_2, H_2O, or CH_4 that diffuse into the electrode from the fuel feed, and J^{e} represents products returning to the fuel channel, due to reforming and electrochemical reactions inside the cell. The terms in the square bracket represent the net enthalpy change associated with reactant moving in and out of the anode, $J^{\text{s}}_{\text{O}_2}\ H_{\text{O}_2}$ is the enthalpy carried by O_2 diffusing to the cell from the air channel. E_{e} is the electrical energy that the cell supplies to the external load, and q_{conv} and q_{rad} are the heat flow due to convection and radiation heat transfer, respectively.

By using the species mass balance around the cell, and considering the reforming reaction at the surface of the electrode within the cell, the energy balance (Eq. 8) can be rearranged and simplified to yield the result of Qi et al.[11]

$$\frac{d\rho_{\text{cell}}C_{p,\text{cell}}T_{\text{cell}}}{dt} = J^{\text{s}}_{\text{H}_2}H_{\text{H}_2} + J^{\text{s}}_{\text{O}_2}H_{\text{O}_2} + J^{\text{s}}_{\text{H}_2\text{O}}H_{\text{H}_2\text{O}} - E_{\text{e}} - q_{\text{conv}} - q_{\text{rad}} - q_{\text{ref}} \quad (9)$$

Here J^{s} represents reactant flows that diffuse to *tpb* to participate in the electrochemical reaction, and $q_{\text{ref}} = r_{\text{ref}} \cdot \Delta H_{\text{ref}}$ the ehthalpy change associated with the reforming reaction.

Converting the mass flow to flux, the dynamic local cell temperature model is

$$\frac{dT_{\text{cell}}}{dt} = \frac{1}{\rho_{\text{cell}}C_{p,\text{cell}}} \cdot \frac{1}{r^*_3} \cdot [j^s_{\text{H}_2}H_{\text{H}_2}|_{T_{\text{fuel}}} + \frac{r_2}{r_3} \cdot j^s_{\text{O}_2}H_{\text{O}_2}|_{T_{\text{air}}} + j^s_{\text{H}_2\text{O}}H_{\text{H}_2\text{O}}|_{T_{\text{cell}}} - (V_{\text{ct}} - \rho_{\text{R}_o}l_{\text{R}_o} \cdot i)i - h_{\text{a}}(T_{\text{cell}} - T_{\text{fuel}}) - \frac{r_2}{r_3} \cdot h_{\text{c}}(T_{\text{cell}} - T_{\text{air}}) - \frac{r_2}{r_3} \cdot \frac{\sigma}{R_{\text{rad}}}(T^4_{\text{cell}} - T^4_{\text{tube}}) - r_{\text{ref}} \cdot \Delta H_{\text{ref}}] \quad (10)$$

where ρ_{cell} and $C_{p,\text{cell}}$ are the density and the heat capacity of the cell, respectively, r_2 and r_3 are the inner and outer radius of the cell, and $r^*_3 = (r^2_3 - r^2_2)/(2r_3)$.

Injection Tube Temperature. The injection tube is a passive component in the heat-transfer process. It exchanges heat with air flows through forced convection, and is heated by the cell through radiation. The dynamics, thus, can be modeled following the similar procedure shown previously

$$\frac{dT_{\text{tube}}}{dt} = \frac{1}{\rho_{\text{tube}}C_{p,\text{tube}}} \cdot \frac{1}{r^*_1} \cdot [-h_{\text{c}}(T_{\text{tube}} - T_{\text{air}}) - \frac{r_0}{r_1} \cdot h_{\text{t}}(T_{\text{tube}} - T_{\text{inj}}) + \frac{r_2}{r_1} \cdot \frac{\sigma}{R_{\text{rad}}}(T^4_{\text{cell}} - T^4_{\text{tube}})] \quad (11)$$

where ρ_{tube} and $C_{p,\text{tube}}$ are the density and the heat capacity of the injection tube, respectively, r_0 and r_1 are inner and outer radius of the injection tube respectively, and $r^*_1 = (r^2_1 - r^2_0)/(2r_1)$

Fuel Flow

In the tubular SOFC stack that we consider, fuel gas is pre-reformed methane, consisting of CH_4, H_2O, H_2, CO, and CO_2. The fuel temperature, velocity and species concentrations etc., are distributed along the flow channel, because of mass, heat and momentum exchange through secondary flow and the reforming/shifting reaction. The dynamics of fuel flow can be described by 1-D equation of continuity, the equation of energy and the equation of motion.

Concentrations. Reforming and shifting reactions generate H_2, CO and CO_2 from methane and steam

$$\text{Reforming}: \quad \text{CH}_4 + \text{H}_2\text{O} \rightleftharpoons 3\text{H}_2 + \text{CO}$$
$$\text{Shift}: \quad \text{CO} + \text{H}_2\text{O} \rightleftharpoons \text{H}_2 + \text{CO}_2$$

The reforming reaction is assumed to occur at the surface of anode. Based on the methane consumption rate, the reforming rate is experimentally determined as[12]

$$r_{\text{ref}} = -r_{\text{CH}_4} = K_{\text{r}}p^{\alpha}_{\text{CH}_4}p^{\beta}_{\text{H}_2\text{O}}\exp\left(-\frac{E_{\text{r}}}{RT_{\text{fuel}}}\right) \quad (12)$$

where K_{r} is the rate coefficient, E_r is activation energy, and α, β are order coefficients for methane and steam respectively.

The shifting reaction is assumed to occur in the fuel bulk. Usually it is considered to be fast, and the rate is approximated through the equilibrium coefficient[11]

$$r_{\text{sft}} = K_{\text{s}}[p_{\text{CO}}p_{\text{H}_2\text{O}}\exp\left(\frac{4276}{T_{\text{fuel}}} - 3.961\right) - p_{\text{CO}_2}p_{\text{H}_2}] \quad (13)$$

where K_{s} is the rate coefficient.

Converting species dynamic models[11] for a finite volume of SOFC to the whole length of the cell, the 1-D species dynamic models are

$$\begin{aligned}
\frac{\partial C_{\text{CH}_4}}{\partial t} &= -\frac{\partial}{\partial z}u_{\text{fuel}}C_{\text{CH}_4} - \frac{1}{r^*} \cdot r_{\text{ref}} \\
\frac{\partial C_{\text{H}_2\text{O}}}{\partial t} &= -\frac{\partial}{\partial z}u_{\text{fuel}}C_{\text{H}_2\text{O}} - \frac{1}{r^*} \cdot r_{\text{ref}} - \frac{1}{r^*} \cdot r_{\text{sft}} - \frac{1}{r^*} \cdot j^{\text{s}}_{\text{H}_2\text{O}} \\
\frac{\partial C_{\text{H}_2}}{\partial t} &= -\frac{\partial}{\partial z}u_{\text{fuel}}C_{\text{H}_2} + 3 \cdot \frac{1}{r^*} \cdot r_{\text{ref}} + \frac{1}{r^*} \cdot r_{\text{sft}} - \frac{1}{r^*} \cdot j^{\text{s}}_{\text{H}_2} \\
\frac{\partial C_{\text{CO}}}{\partial t} &= -\frac{\partial}{\partial z}u_{\text{fuel}}C_{\text{CO}} + \frac{1}{r^*} \cdot r_{\text{ref}} - \frac{1}{r^*} \cdot r_{\text{sft}} \\
\frac{\partial C_{\text{CO}_2}}{\partial t} &= -\frac{\partial}{\partial z}u_{\text{fuel}}C_{\text{CO}_2} + \frac{1}{r^*} \cdot r_{\text{sft}}
\end{aligned} \quad (14)$$

where $r^* = \frac{4-\pi}{2\pi} r_3$ is geometry fitness parameter, and u_{fuel} the local fuel velocity.

Temperature. The fuel temperature is affected by several factors: reforming and shifting reactions, enthalpies that are carried by reactant fluxes, and heat transferred from its surroundings, etc. The effect of kinetic energy can be neglected due to low velocity and low density.

So the 1-D temperature dynamic model is converted from the dynamic fuel temperature model[11]

$$\frac{\partial}{\partial t}\left(\sum (C_i C_{p,i}) \cdot T_{\text{fuel}}\right) = -\frac{\partial}{\partial z}\left(u_{\text{fuel}} \sum (C_i H_i)\right) - \frac{1}{r^*} \cdot j^{\text{s}}_{\text{H}_2} H_{\text{H}_2} - \frac{1}{r^*} \cdot j^{\text{s}}_{\text{H}_2\text{O}} H_{\text{H}_2\text{O}} - \frac{1}{r^*} \cdot h_{\text{a}}(T_{\text{fuel}} - T_{\text{cell}}) + \frac{1}{r^*} \cdot r_{\text{ref}} \cdot \Delta H_{\text{ref}} \quad (15)$$

where C_i's are concentrations of each species in the fuel gas, $C_{p,i}$ their specific heats at constant pressure, and H_i enthalpy of formations.

Velocity. The flow velocity determines space time in the fuel channel and affects the heat transfer coefficient; thus, it is the dominant factor that affects concentrations and the temperature.

In the fuel channel, the reforming/shifting reactions, and the electrochemical reaction induce pressure gradient, and, thus, affect forces acting on the primary flow and, consequently, the velocity. Because the density of gas-flow is small, the pressure gradient that will produce forces to accelerate the gas-flow body to reach a equilibrium velocity is very small. The pressure distribution, therefore, can be assumed uniform along the channel, and this assumption will be used in the later discussion for analytical solution.

In addition, due to the electrochemical reaction, some H_2 in the fuel flow is exchanged by H_2O through secondary flow, leading density change, thus, the velocity change. The effect of friction is minor and can be neglected because of the small viscosity of fuel.

The dynamic behaviors of flow velocities were modeled in the 1-D form

$$\frac{\partial}{\partial t}\left(\sum (C_i M_i) \cdot u_{\text{fuel}}\right) = -\frac{\partial}{\partial z}\left(\sum \left(C_i M_i \cdot u^2_{\text{fuel}}\right)\right) - \frac{1}{r^*} \cdot j^{\text{s}}_{\text{H}_2} M_{\text{H}_2} u_{\text{fuel}} - \frac{\partial P_{\text{fuel}}}{\partial z} \quad (16)$$

where M_i's are mole masses of each species.

Air flow

Air is injected to the bottom of the cell tube, and then turns around and goes through the gap formed by the cell and the injection tube. So airflow is divided into two sections. In the cathode channel, air is coflow with fuel, and O_2 diffuses into the cathode. In the injection channel, air is counterflow relative to the fuel-flow, and no reaction or secondary flow occurs.

Cathode Channel Air Flow. We assume that air consists of N_2 and O_2 only. N_2 is not involved in any reactions, and only O_2 diffuses into the cell to participate in the electrochemical reaction. The airflow exchanges heat with the cell tube and the injection tube, respectively, and affects the velocity. The 1-D species dynamics, temperature dynamics and velocity dynamics are

$$\frac{\partial C_{\text{N}_2}}{\partial t} = -\frac{\partial}{\partial z} u_{\text{air}} C_{\text{N}_2}$$
$$\frac{\partial C_{\text{O}_2}}{\partial t} = -\frac{\partial}{\partial z} u_{\text{air}} C_{\text{O}_2} - \frac{1}{r^*_2} \cdot j^{\text{s}}_{\text{O}_2} \quad (17)$$

$$\frac{\partial}{\partial t}\left(\sum (C_j C_{p,j}) \cdot T_{\text{air}}\right) = -\frac{\partial}{\partial z}\left(u_{\text{air}} \sum (C_j H_j)\right) - \frac{1}{r^*_2} \cdot j^{\text{s}}_{\text{O}_2} H_{\text{O}_2} - \frac{1}{r^*_2} \cdot h_{\text{c}}(T_{\text{air}} - T_{\text{cell}}) - \frac{1}{r^*_2} \cdot \frac{r_1}{r_2} \cdot h_{\text{c}}(T_{\text{air}} - T_{\text{tube}}) \quad (18)$$

$$\frac{\partial}{\partial t}\left(\sum (C_j M_j) \cdot u_{\text{air}}\right) = -\frac{\partial}{\partial z}\left(\sum (C_j M_j \cdot u^2_{\text{air}})\right) - \frac{1}{r^*_2} \cdot j^{\text{s}}_{\text{O}_2} M_{\text{O}_2} u_{\text{air}} - \frac{\partial P_{\text{air}}}{\partial z} \quad (19)$$

where $r^*_2 = (r_2^2 - r_1^2)/(2r_2)$ is the geometry adjustment parameter, C_j's are concentrations of N_2 and O_2, $C_{p,j}$ their specific heat, H_j their enthalpy of formations, and h_c the cathode side heat-transfer coefficient, which is affected by the velocity.[11]

Injection Channel Airflow. In the injection tube, except for the primary flow, the airflow only exchanges heat with the tube; no other transport processes occur. The flow direction is opposite to the axial direction, as shown in Figure 1. In the 1-D modeling, the location of the airflow in the injection channel is represented by y instead of z. They have the relation $y = L - z$.

We are only interested in the temperature dynamics for the airflow in the injection tube. Species concentrations and the velocity are assumed to be the same as that at the inlet. The temperature can then be modeled by

$$C^{\text{in}}_{\text{air}} C_{p,\text{air}} \cdot \frac{\partial T_{\text{inj}}}{\partial t} = -u^{\text{in}}_{\text{air}} C^{\text{in}}_{\text{air}} \cdot \frac{\partial H_{\text{air}}}{\partial y} - \frac{r_0}{2} \cdot h_{\text{t}}(T_{\text{inj}} - T_{\text{tube}}) \quad (20)$$

where $C^{\text{in}}_{\text{air}}$ is the air concentration at the inlet, $C_{p,\text{air}}$ the air specific heat at constant pressure, $u^{\text{in}}_{\text{air}}$ the input velocity, and h_{t} the heat-transfer coefficient, which is affected by the velocity.

Approximate Analytical Solution

An 1-D dynamic model is usually solved through numerical methods. The fundamental approach of numerical methods is discretization of the continuous model. Employing numerical methods, the number of equations to be solved increases quickly. For a complex system, such as SOFC, over twenty variables are modeled in the form of nonlinear, non-homogeneous PDEs. This results in heavy computations if numerical approaches are adopted. Therefore, numerical methods may not be suitable for certain real-time applications, such as control applications.

In control applications, to meet online computation requirement, the system model is often simplified. Fast dynamics can be approximated by steady-state solution;[9] nondominant dynamic variables may be neglected;[3] distributed parameter system can be lumped to give a set of ordinary differential equations.[13] The objective is to reduce the computation requirement. However, these simplifications unavoidably induce large model errors.

Clearly, an analytical solution can satisfy both speed and precision requirements. However, it is very difficult, if not

impossible, to find exact analytical solutions for those nonlinear, non-homogeneous and coupled PDEs, such as the 1-D dynamic model of SOFC. In this section, aiming at solving the 1-D reacting gas-flow problem, we attempt to develop an approximated analytical solution that can balance the speed and precision requirements.

Problem description

Analysis in the previous section has shown that the model of SOFC mainly consists of two parts: the nonflowing phase part and the flowing phase part. Parameter distributions of nonflowing phase also depend on that of the flowing phase. In the SOFC stack that we are considering, the flowing phase consists of three primary flow bodies: fuel-flow, airflow in the cathode channel, and airflow in the injection tube. The fuel-flow is the most representative one, and it is used as an example for the 1-D reacting gas-flow problem in the following development.

Within the primary flow, the mixed gases are reacting. So concentrations of each species are not constant along the flow channel, and the total concentration is affected by the reaction. Simultaneously, the primary flow exchanges heat with the wall of the flow channel. The change of the gas-phase temperature, thus, leads to pressure change. The pressure gradient induced by the reaction and the temperature significantly affects the primary flow velocity. Through the secondary flow, H_2 in the primary flow body gradually changes to H_2O. The density of the mixture is thus changed. This in turn affects the primary flow velocity.

A flow body can be described by three distributed variables: concentrations, energy, and velocity. Their dynamic behaviors can be modeled by several PDEs, as shown by Eq. 14, 15 and 16. In general, the dynamic 1-D model for a reacting gas flow can be written as

$$\begin{aligned} \frac{\partial C_i}{\partial t} &= -\frac{\partial}{\partial z}(uC_i) + \mathcal{A} \\ &\vdots \\ \frac{\partial}{\partial t}CC_pT &= -\frac{\partial}{\partial z}(uCH) + \mathcal{B} \\ \frac{\partial}{\partial t}CMu &= -\frac{\partial}{\partial z}(CMu^2) - \frac{\partial P}{\partial z} + \mathcal{C} \end{aligned} \tag{21}$$

where C is the total concentration, u the velocity, H enthalpy of formation, T the temperature, and $\mathcal{A}, \mathcal{B}, \mathcal{C}$ combinations of nonhomogeneous terms, respectively.

Strict analytical solution for this model is beyond our scope. We shall derive an approximate solution in the form of Eq. 1.

Assumptions

As we have analyzed before, the 1-D reacting gasflow has the following characteristics:

- Reaction leading to total mole number change;
- Heat exchange leading to temperature change;
- Momentum change;
- Constant flow area;
- Frictionless;
- Velocity lower than 0.3 Mach.

Obviously, gas-phase fluid is compressible, especially when considering its dynamics. However, the knowledge of gas dynamics also shows that when the flow velocity is lower than 0.3 Mach, gas can be assumed incompressible.[14] That is, for the gas-phase fluid, its pressure can be assumed uniform along the flow channel if we neglect the friction, as we discussed previously. Numerical simulations from the detailed model shown by Eq. 21 support this assumption.[9] So, according to the law of mass conservation, the velocity is distributed due to the mole number change led by the reaction. In this case, the velocity is mainly determined by the continuity. The effect of momentum change is minor and may be neglected. Gas dynamics also shows that the dynamic response of velocity to inlet disturbance is very fast. The state changes only occur within a very thin layer named shock wave. The shock wave moves fast, in the sonic speed.[14] So, with the condition that the flow channel is not long, the velocity dynamics can be neglected. Therefore, in order to develop the analytical solution, we make the following assumptions:

- Gas-phase flow is incompressible;
- Pressure along the flow channel is uniform;
- Velocity is distributed due to reaction;
- The effect of density change can be neglected;
- Velocity dynamics can be neglected.

Approximated analytical solution

Velocity. Since velocity is the dominant variable of the fluid, and it is considered at steady state, the key to obtaining an approximate analytical solution starts from the solution of the velocity.

For the fuel-flow, continuity equations are shown in Eq. 14. Dividing them by the total concentration C, concentrations of each species can be converted to mole fractions

$$\begin{aligned} \frac{\partial \chi_{CH_4}}{\partial t} &= -\frac{\partial}{\partial z}u_{\text{fuel}}\chi_{CH_4} - \frac{1}{r^*}\cdot\frac{1}{C}r_{\text{ref}} \\ \frac{\partial \chi_{H_2O}}{\partial t} &= -\frac{\partial}{\partial z}u_{\text{fuel}}\chi_{H_2O} - \frac{1}{r^*}\cdot\frac{1}{C}r_{\text{ref}} - \frac{1}{r^*}\cdot\frac{1}{C}r_{\text{sft}} - \frac{1}{r^*}\cdot\frac{1}{C}j^{\text{s}}_{H_2O} \\ \frac{\partial \chi_{H_2}}{\partial t} &= -\frac{\partial}{\partial z}u_{\text{fuel}}\chi_{H_2} + \cdot\frac{1}{r^*}\cdot\frac{3}{C}r_{\text{ref}} + \frac{1}{r^*}\cdot\frac{1}{C}r_{\text{sft}} - \frac{1}{r^*}\cdot\frac{1}{C}j^{\text{s}}_{H_2} \\ \frac{\partial \chi_{CO}}{\partial t} &= -\frac{\partial}{\partial z}u_{\text{fuel}}\chi_{CO} + \frac{1}{r^*}\cdot\frac{1}{C}r_{\text{ref}} - \frac{1}{r^*}\cdot\frac{1}{C}r_{\text{sft}} \\ \frac{\partial \chi_{CO_2}}{\partial t} &= -\frac{\partial}{\partial z}u_{\text{fuel}}\chi_{CO_2} + \frac{1}{r^*}\cdot\frac{1}{C}r_{\text{sft}} \end{aligned} \tag{22}$$

Summing them up yields

$$\frac{\partial}{\partial t}\sum\chi_i = -\frac{\partial}{\partial z}u_{\text{fuel}}\sum\chi_i + \frac{1}{r^*}\cdot\frac{2}{C}r_{\text{ref}} - \frac{1}{r^*}\cdot\frac{1}{C}j^{\text{s}}_{H_2O} - \frac{1}{r^*}\cdot\frac{1}{C}j^{\text{s}}_{H_2} \tag{23}$$

Note obvious identities

$$\sum\chi_i = 1; \quad \frac{d1}{dt} = 0; \quad \text{and} \quad \frac{d1}{dz} = 0$$

For SOFC, we have $j^{\text{s}}_{H_2} = -j^{\text{s}}_{H_2O}$.

Substituting these equations into Eq. 23, and rearranging gives

$$\frac{du_{\text{fuel}}}{dz} = \frac{1}{r^*} \cdot \frac{2}{C} r_{\text{ref}}$$

B.C.

$$\begin{aligned} u_{\text{fuel}} &= u_{\text{fuel}}^{\text{in}}; \quad \text{at } z = 0 \\ C &= C^{\text{in}}; \quad \text{at } z = 0 \\ r_{\text{ref}} &= r_{\text{ref}}^{\text{in}}; \quad \text{at } z = 0 \end{aligned} \tag{24}$$

This result shows that the velocity distribution depends on the reaction rate in SOFC anode fuel flow.

Since the distribution of r_{ref} and the total concentration C are affected by other variables and are not constants, direct integration of u_{fuel} is not possible. The velocity at location z can be integrated approximately from Eq. 24, using different approximation methods, such as the Trapezoidal approximation, according to preknowledge of the r_{ref} profile.

With the approximated solution for steady-state velocity at location z, we avoid the need of the equation of momentum balance.

Decoupling. Due to the terms of concentrations, the temperature and the velocity affect each other. For a gas-flow, the equation of continuity, the equation of energy, and the equation of motion are coupled, as shown by Eq. 21. They should be decoupled in order to find the analytical solution.

Physically, although reactions and the mass transfer within secondary flow affect concentrations of each species, they are dominated by the primary flow itself. That is, the equation of continuity is dominated by the term $\frac{\partial}{\partial z}(uC_i)$. So in solving the continuity equation, we can assume that other factors, such as temperature are constant.

For the energy equation, the temperature is dominated by flow velocity and energy exchanges. The change of concentration actually has only minor effects on the dynamic response process. It does not affect the terminal temperature value. So concentration in the energy equation can be seen as constant.

With these two assumptions and the velocity equation developed previously, the equation of continuity, and the equation of energy can be resolved independently. This is the principle behind decoupling in the following derivation.

Analytical Solution. In general, the 1-D dynamic reacting gas-flow model can be simplified to the form of

$$\begin{aligned} &\frac{\partial v}{\partial t} = -a \cdot u \cdot \frac{\partial v}{\partial z} - b \cdot v - c; \\ &\text{Assume:} \quad u = A + B \cdot z \\ &\text{With} \\ &\text{B.C.}: \quad v = v^{\text{in}} \quad \text{at} \quad z = 0; \\ &\text{I.C.}: \quad v = v^0 \quad \text{at} \quad t = 0; \end{aligned} \tag{25}$$

where v is the interested physical variable, u the velocity, and a, b, c, A and B coefficients.

Performing Laplace transform to the PDE in terms of time t, it can be converted to an ODE

$$\begin{aligned} sv - v^0 &= -a \cdot u \cdot \frac{\partial v}{\partial z} - b \cdot v - c \\ u &= A + B \cdot z \\ \text{B.C.}: \quad v &= v^{\text{in}} \quad \text{at} \quad z = 0 \end{aligned} \tag{26}$$

where s is the Laplace operator.

The ODE shown in Eq. 26 can be analytically solved

$$sv - v^0 = -bv - c + [bv^{\text{in}} + c + (sv^{\text{in}} - v^0)] \cdot \left(1 + \frac{B}{A} \cdot z\right)^{-\frac{b+s}{aB}} \tag{27}$$

Neglecting the effect of inlet transient process, and performing inverse Laplace transform, the result can then be transferred to ODE with respect to time t again

$$\frac{dv}{dt} = -bv - c + (bv^{\text{in}} + c) \cdot \left(1 + \frac{B}{A} z\right)^{-\frac{b}{aB}} \tag{28}$$

This is the approximated analytical solution for 1-D dynamic reacting gas-flow problem, when the velocity distribution profile can be approximated linearly.

Application to SOFC

Numerical simulations show that the profile of r_{ref} under the given condition has an exponential like shape,[15] so first-order approximation of the velocity u as shown in Eq. 25, will lead to large error when z increases. A more accurate approximation needs to be developed.

Reforming rate and velocity

Assume that the distribution of r_{ref} can be approximated by

$$r_{\text{ref}} = r^{\text{in}} \exp\left(-\frac{z}{\xi}\right) \tag{29}$$

We need to find the space constant ξ.

The reforming reaction rate of Eq. 12 shows that r_{ref} is proportional to $p_{\text{CH}_4}^{0.85}$, and may be approximated by Kp_{CH_4} for the sake of possible analytical solution. Substituting this approximation into the steady-state equation of continuity, and rearranging it to the form of mole fraction we get

$$\frac{\partial}{\partial z} u\chi_{\text{CH}_4} = -\frac{K}{r^* C} \chi_{\text{CH}_4} \tag{30}$$

Obviously, the space constant of χ_{CH_4} is

$$\xi = \frac{r^* C u^{\text{in}}}{K} \tag{31}$$

where $K = r_{\text{ref}}^{\text{in}} / \chi_{\text{CH}_4}^{\text{in}}$. It equals to the space constant of r_{ref}.

So the steady-state velocity can be analytically integrated from the r_{ref} approximation in Eq. 29

$$u = u^{\text{in}} + \frac{2}{r^* C} r^{\text{in}} \xi \cdot \left[1 - \exp\left(-\frac{z}{\xi}\right)\right] \tag{32}$$

Analytical solution

Therefore, the reacting gas-flow problem in SOFC can be concluded as

$$\begin{aligned}\frac{\partial v}{\partial t} &= -\frac{\partial}{\partial z}uv + b(z) + c;\\ u &= A + B\cdot\left[1-\exp\left(-\frac{z}{\xi}\right)\right];\end{aligned} \tag{33}$$

With

$$\text{B.C.}: \; v = v^{\text{in}} \quad \text{at} \quad z = 0;$$
$$\text{I.C.}: \; v = v^{0} \quad \text{at} \quad t = 0;$$

Converting the PDE to an ODE by performing Laplace transform in terms of time t

$$sv - v^0 = -u\frac{dv}{dz} - v\frac{du}{dz} + b(z) + c \tag{34}$$

It can be rearranged as

$$(u+sz)\cdot\frac{dv}{dz} + \left(\frac{du}{dz}+s\right)\cdot v - sz\cdot\frac{dv}{dz} = b(z) + c + v^0 \tag{35}$$

The position z in the axial coordinate is independent of time t, so sz equals to zero, and the term $sz\cdot\frac{dv}{dz}$ can be removed from the equation. The ODE can then be shown as

$$a_1(z)\frac{dv}{dz} + a_0(z)v = b(z) + c + v^0$$

with $a_1'(z) = a_0(z)$. This equation can be solved through

$$a_1(z)v = \int (b(z) + c + v^0)dz$$

Knowing $b(z) = \frac{n}{r^*C}r_{\text{ref}}$, the solution is

$$(u+sz)v = u^{\text{in}}v^{\text{in}} - uv + \frac{n}{r^*C}r^{\text{in}}\xi\cdot\left[1-\exp\left(-\frac{z}{\xi}\right)\right] + (c+v^0)\cdot z \tag{36}$$

Performing inverse Laplace transform and rearranging the equation we get

$$\frac{dv}{dt} = \frac{1}{z}\cdot\left[u^{\text{in}}v^{\text{in}} - uv + \frac{n}{r^*C}r^{\text{in}}\xi\cdot\left[1-\exp\left(-\frac{z}{\xi}\right)\right] + c\cdot z\right] \tag{37}$$

Application

Applying the solution shown by Eq. 37 to the SOFC fuel-flow, distributed dynamic models of specie mole fractions are:

$$\frac{d\chi_{\text{CH}_4}}{dt} = \frac{1}{z\cdot r^*}\cdot\frac{RT_{\text{fuel}}}{P^{\text{in}}_{\text{fuel}}}\cdot\left\{-u_{\text{fuel}}\chi_{\text{CH}_4} + u^{\text{in}}_{\text{fuel}}\chi^{\text{in}}_{\text{CH}_4} - r^{\text{in}}_{\text{ref}}\xi\left[1-\exp\left(-\frac{z}{\xi}\right)\right]\right\} \tag{38}$$

$$\frac{d\chi_{\text{H}_2\text{O}}}{dt} = \frac{1}{z\cdot r^*}\cdot\frac{RT_{\text{fuel}}}{P^{\text{in}}_{\text{fuel}}}\cdot\left\{-u_{\text{fuel}}\chi_{\text{H}_2\text{O}} + u^{\text{in}}_{\text{fuel}}\chi^{\text{in}}_{\text{H}_2\text{O}} - r^{\text{in}}_{\text{ref}}\xi\left[1-\exp\left(-\frac{z}{\xi}\right)\right] + (-r_{\text{sft}} - j^{\text{s}}_{\text{H}_2\text{O}})z\right\} \tag{39}$$

$$\frac{d\chi_{\text{H}_2}}{dt} = \frac{1}{z\cdot r^*}\cdot\frac{RT_{\text{fuel}}}{P^{\text{in}}_{\text{fuel}}}\cdot\left\{-u_{\text{fuel}}\chi_{\text{H}_2} + u^{\text{in}}_{\text{fuel}}\chi^{\text{in}}_{\text{H}_2} + 3r^{\text{in}}_{\text{ref}}\xi\left[1-\exp\left(-\frac{z}{\xi}\right)\right] + (r_{\text{sft}} - j^{\text{s}}_{\text{H}_2\text{O}})z\right\} \tag{40}$$

$$\frac{d\chi_{\text{CO}}}{dt} = \frac{1}{z\cdot r^*}\cdot\frac{RT_{\text{fuel}}}{P^{\text{in}}_{\text{fuel}}}\cdot\left\{-u_{\text{fuel}}\chi_{\text{CO}} + u^{\text{in}}_{\text{fuel}}\chi^{\text{in}}_{\text{CO}} + r^{\text{in}}_{\text{ref}}\xi\left[1-\exp\left(-\frac{z}{\xi}\right)\right] - r_{\text{sft}}\cdot z\right\} \tag{41}$$

$$\frac{d\chi_{\text{CO}_2}}{dt} = \frac{1}{z\cdot r^*}\cdot\frac{RT_{\text{fuel}}}{P^{\text{in}}_{\text{fuel}}}\left\{-u_{\text{fuel}}\chi_{\text{CO}_2} + u^{\text{in}}_{\text{fuel}}\chi^{\text{in}}_{\text{CO}_2} + r_{\text{sft}}\cdot z\right\} \tag{42}$$

where z is the location.

In solving the fuel temperature model in Eq. 15, assume that specie gradients are zero; therefore, the term $r_{\text{ref}}\ \Delta H_{\text{ref}}$ should be removed. Instead, the term that represents the shifting reaction heat $r_{\text{sft}}\Delta H_{\text{sft}}$ should be considered in the equation. In addition, the total concentration C, the specific heat $C_{p,\text{fuel}}$ and the velocity u are also assumed constant since the effect of their gradients on the temperature is minor. The enthalpy of formation is approximated by first-order polynomials of temperature, in the form of $H = a + b\cdot T$.[11] So using the trapezoidal approximation of velocity distribution, the approximate analytical solution of the fuel temperature is

$$\begin{aligned}\frac{dT_{\text{fuel}}}{dt} = \frac{1}{r^*C_{p,\text{fuel}}}\cdot\frac{RT_{\text{fuel}}}{P^{\text{in}}_{\text{fuel}}}\cdot\Big\{&-j^{\text{s}}_{\text{H}_2}(a_{\text{H}_2} + b_{\text{H}_2}T_{\text{fuel}})\\ &- h_{\text{a}}(T_{\text{fuel}} - T_{\text{cell}}) - j^{\text{s}}_{\text{H}_2\text{O}}(a_{\text{H}_2\text{O}} + b_{\text{H}_2\text{O}}T_{\text{cell}}) + r_{\text{sft}}\Delta H_{\text{sft}}\\ &+ \Big[j^{\text{s}}_{\text{H}_2}(a_{\text{H}_2} + b_{\text{H}_2}T^{\text{in}}_{\text{fuel}}) + h_{\text{a}}(T^{\text{in}}_{\text{fuel}} - T_{\text{cell}})\\ &+ j^{\text{s}}_{\text{H}_2\text{O}}(a_{\text{H}_2\text{O}} + b_{\text{H}_2\text{O}}T_{\text{cell}}) - r_{\text{sft}}\Delta H_{\text{sft}}\Big]\\ &\cdot\exp\left(-\frac{1}{r^*}\cdot\frac{RT_{\text{fuel}}}{P^{\text{in}}_{\text{fuel}}}\cdot\frac{j^{\text{s}}_{\text{H}_2}b_{\text{H}_2} + h_{\text{a}}}{u_{\text{fuel}}\chi_i b_i}\cdot z\right)\Big\}\end{aligned} \tag{43}$$

The velocity distribution of fuel-flow is given by Eq. 32.

For the cathode-side channel, the linearly approximation of u is adopted. Applying the solution shown by Eq. 28 to the cathode side airflow, the distributed dynamic model of O_2 mole fraction is

$$\frac{d\chi_{\text{O}_2}}{dt} = \frac{1}{r_2^*}\cdot\frac{RT_{\text{air}}}{P^{\text{b}}_{\text{air}}}\cdot\left\{-(1-\chi_{\text{O}_2})j^{\text{s}}_{\text{O}_2} + (1-\chi^{\text{b}}_{\text{O}_2})j^{\text{s}}_{\text{O}_2}\left[1-\frac{1}{2r_2^*}\cdot\frac{R}{P^{\text{b}}_{\text{air}}u^{\text{b}}_{\text{air}}}\cdot(T^{\text{b}}_{\text{air}} + T_{\text{air}})j^{\text{s}}_{\text{O}_2}\cdot z\right]^{-2\frac{T_{\text{air}}}{T^{\text{b}}_{\text{air}}+T_{\text{air}}}}\right\} \tag{44}$$

where $P^{\text{b}}_{\text{air}} = P^{\text{in}}_{\text{air}}$, $u^{\text{b}}_{\text{air}} = \frac{r_0}{r_2 - r_1}u^{\text{in}}_{\text{air}}$, and $T^{\text{b}}_{air} = T_{\text{inj}}|_{z=0}$ are airflow parameters at the close end of the tube.

The distributed dynamic air temperature model is

$$\begin{aligned}\frac{dT_{\text{air}}}{dt} = \frac{1}{r_2^*C_{p,\text{air}}}\cdot\frac{RT_{\text{air}}}{P^{\text{b}}_{\text{air}}}\cdot\Big\{&-(h_{\text{c}} + \frac{r_1}{r_2}h_{\text{c}})T_{\text{air}}\\ &- (-h_{\text{c}}T_{\text{cell}} + \frac{r_1}{r_2}h_{\text{c}}T_{\text{tube}}) + \Big[(h_{\text{c}} + \frac{r_1}{r_2}h_{\text{c}})T^{\text{b}}_{\text{air}}\\ &+ (-h_{\text{c}}T_{\text{cell}} + \frac{r_1}{r_2}h_{\text{c}}T_{\text{tube}})\Big]\left[1-\frac{1}{2r_2^*}\cdot\frac{R}{P^{\text{b}}_{\text{air}}u^{\text{b}}_{\text{air}}}\right.\\ &\left.\cdot\,(T^{\text{b}}_{\text{air}} + T_{\text{air}})j^{\text{s}}_{\text{O}_2}\cdot z\right]^{-2\frac{T_{\text{air}}}{T^{\text{b}}_{\text{air}}+T_{\text{air}}}}\Big\}\end{aligned} \tag{45}$$

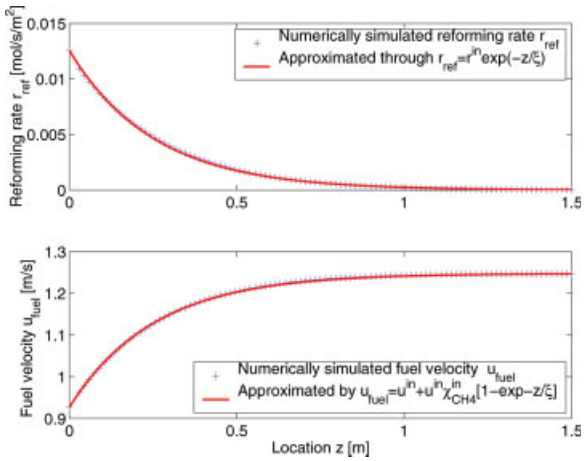

Figure 4. Comparison of numerically simulated and the approximate analytical solution of reforming reaction rate and fuel velocity profiles.

[Color figure can be viewed in the online issue, which is available at www.interscience.wiley.com.]

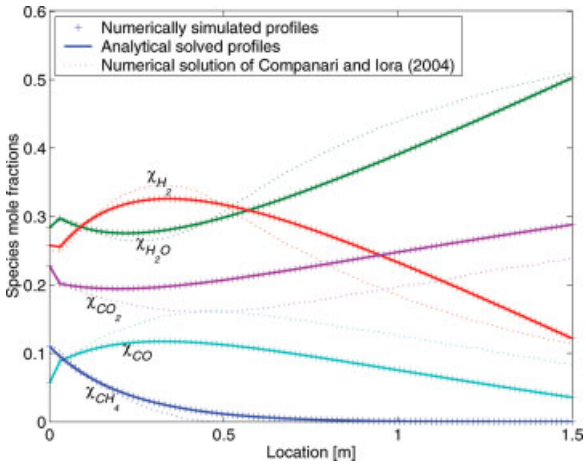

Figure 5. Comparison of numerically simulated and the approximate analytical solution of species mole fraction profiles.

Parameters: I = 150A, P_{fuel} = 1.036atm, T_{fuel} = 923K, u^{in}_{fuel} = 0.974m/s. [Color figure can be viewed in the online issue, which is available at www.interscience.wiley.com.]

The velocity distribution is

$$u_{air} = u^{b}_{air} - \frac{1}{2r_2^*}\cdot\frac{R}{P^{b}_{air}}(T^{b}_{air}+T_{air})\cdot j^{s}_{O_2}\cdot z \tag{46}$$

We are also interested in the temperature of airflow inside the injection tube

$$\frac{dT_{inj}}{dt} = \frac{2}{r_0 C_{p,air}}\cdot\frac{RT_{inj}}{P^{in}_{air}}\cdot\left\{-h_t T_{inj} + h_t T_{tube} + (h_t T^{in}_{air} - h_t T_{tube})\cdot\exp\left[-\frac{2}{r_2}\cdot\frac{R}{P^{in}_{air}u^{in}_{air}}\cdot\frac{h_t}{b_{air}}T_{inj}\cdot(L-z)\right]\right\} \tag{47}$$

Steady-state verification

The approximate analytical solution of fuel-gas profiles, and numerical simulations are compared, as shown in Figures. 4 and 5, respectively. Lines with a cross mark are numerically simulated profiles from Eq. 14. Solid lines are the approximate analytical solution results, directly from Eq. 38, 39, 40, 41, and 42. Simulation shows that the approximate solution Eq. 37 has good precision for this application.

It also shows in Figure 5 that under same input condition, the overall trends of the developed model are consistent with the numerical simulation results in the literature.[15] The differences is mainly induced by the fuel temperature distribution. In our model, we considered not only the effect of convection, but also the effect of radiation, the effect of reforming/shifting reaction, and the effect of enthalpy change with mass exchange. The fuel temperature distribution, is, therefore, different than that shown in the literature.[15] The equilibrium of the shifting reaction is consequently different, and leads to the differences of species distribution profile.

State-Space Model

Assembling dynamic models for each physical variables previously shown, the dynamic model at any location of the SOFC stack can be described in the form of a nonlinear state-space model.

For the SOFC stack we are considering, physical variables that can be manipulated at the entrance are designated as inputs. Their perturbations affect the dynamic performance of the SOFC stack. Intermediate variables are designated as state variables. The electrical output of the stack is the output variable, and other interested variables that can be measured can also be designed as model output. The location z in the stack and other variables, such as mole fractions in the inlet flow are considered as parameters.

So the input vector $\mathbf{u}$ is defined as

$$\mathbf{u} = \begin{bmatrix} I & P^{in}_{fuel} & T^{in}_{fuel} & u^{in}_{fuel} & P^{in}_{air} & T^{in}_{air} & u^{in}_{air} \end{bmatrix}^T \tag{48}$$

where I is the total external current load demand.

The output vector is

$$\mathbf{y} = \begin{bmatrix} V_{out} & T^{exit}_{fuel} & u^{exit}_{fuel} & T^{exit}_{air} & u^{exit}_{air} & \chi^{exit}_{H_2} & \chi^{exit}_{CO} & \chi^{exit}_{O_2} \end{bmatrix}^T \tag{49}$$

The state vector is defined as

$$\mathbf{x} = \begin{bmatrix} V_{ct} & j^{s}_{H_2} & \dot{j}^{s}_{H_2} & j^{s}_{O_2} & \dot{j}^{s}_{O_2} & j^{s}_{H_2O} & \dot{j}^{s}_{H_2O} & p^{tpb}_{H_2} & \dot{p}^{tpb}_{H_2} & p^{tpb}_{O_2} \\ \dot{p}^{tpb}_{O_2} & p^{tpb}_{H_2O} & \dot{p}^{tpb}_{H_2O} & v_I & T_{cell} & T_{tube} & T_{fuel} & T_{air} & T_{inj} \\ & & & \chi_{CH_4} & \chi_{H_2O} & \chi_{H_2} & \chi_{CO} & \chi_{CO_2} & \chi_{O_2} \end{bmatrix}^T \tag{50}$$

where v_I is the intermediate variable to approximate the derivative of the current input.[10]

A second-order process

$$\frac{d^2v}{dt^2} = f(v)$$

can be expressed by two first-order processes

$$\frac{dv}{dt} = \dot{v}$$
$$\frac{d\dot{v}}{dt} = f(v)$$

Applying this result to models shown by Eqs. 6 and 7, and combining electrical model Eq. 3, physical models shown by Eqs. 10, 11, 43, 45, 47, 38, 39, 40, 41, 42, and 44, the state-space model can be expressed as

States:

$$\dot{x}_1 = \frac{1}{\rho_R \rho_C} E - \frac{1}{\rho_R \rho_C} x_1 - \frac{1}{\rho_C} \frac{u_1}{2\pi r_3 L}$$

$$\dot{x}_2 = x_3$$

$$\dot{x}_3 = -h_1 x_2 - h_2 x_3 + h_1 \frac{1}{2F} \frac{u_1}{2\pi r_3 L} + h_3 \frac{1}{Rx_{17}} (\dot{u}_2 x_{22} + u_2 \dot{x}_{22})$$

$$\dot{x}_4 = x_5$$

$$\dot{x}_5 = -o_1 x_4 - o_2 x_5 + o_1 \frac{1}{4F} \frac{u_1}{2\pi r_3 L} + o_3 \frac{1}{Rx_{18}} (\dot{u}_5 x_{25} + u_5 \dot{x}_{25})$$

$$\dot{x}_6 = x_7$$

$$\dot{x}_7 = -w_1 x_6 - w_2 x_7 + w_1 \frac{1}{2F} \frac{-u_1}{2\pi r_3 L} + w_3 \frac{1}{Rx_{17}} (\dot{u}_2 x_{21} + u_2 \dot{x}_{21})$$

$$\dot{x}_8 = x_9$$

$$\dot{x}_9 = -h_1 x_8 - h_2 x_9 - h_4 \frac{Rx_{15}}{2F} \frac{u_1}{2\pi r_3 L} + h_1 u_2 x_{22} - \frac{4}{l_a} \frac{Rx_{15}}{2F} \left(\frac{Ku_1}{2\pi r_3 L} - x_{14} \right)$$

$$\dot{x}_{10} = x_{11}$$

$$\dot{x}_{11} = -o_1 x_{10} - o_2 x_{11} - o_4 \frac{Rx_{15}}{4F} \frac{u_1}{2\pi r_3 L} + o_1 u_5 x_{25} - \frac{4}{l_c} \frac{Rx_{15}}{4F} \left(\frac{Ku_1}{2\pi r_3 L} - x_{14} \right)$$

$$\dot{x}_{12} = x_{13}$$

$$\dot{x}_{13} = -w_1 x_{12} - w_2 x_{13} - w_4 \frac{Rx_{15}}{2F} \frac{-u_1}{2\pi r_3 L} + w_1 u_2 x_{21} - \frac{4}{l_a} \frac{Rx_{15}}{2F} \left(\frac{-Ku_1}{2\pi r_3 L} + x_{14} \right)$$

$$\dot{x}_{14} = K^2 \frac{u_1}{2\pi r_3 L} - K x_{14}$$

$$\dot{x}_{15} = \frac{1}{r_3^* \rho_{cell} C_{p,cell}} \left[x_2 (a_{H_2} + b_{H_2} x_{17}) + \frac{r_2}{r_3} x_4 (a_{O_2} + b_{O_2} x_{18}) + x_6 (a_{H_2O} + b_{H_2O} x_{17}) - x_1 \frac{u_1}{2\pi r_3 L} - h_a (x_{15} - x_{17}) - \frac{r_2}{r_3} h_c (x_{15} - x_{18}) - \frac{r_2}{r_3} \frac{\sigma}{R_{rad}} (x_{15}^4 - x_{16}^4) - r_{ref} \Delta H_{ref} \right]$$

$$\dot{x}_{16} = \frac{1}{r_1^*} \frac{1}{\rho_{tube} C_{p,tube}} \left[-h_c (x_{16} - x_{18}) - \frac{r_0}{r_1} h_t (x_{16} - x_{19}) + \frac{r_2}{r_1} \frac{\sigma}{R_{rad}} (x_{15}^4 - x_{16}^4) \right]$$

$$\dot{x}_{17} = \frac{1}{r^*} \frac{1}{C_{p,fuel}} \frac{Rx_{17}}{u_2} \Big\{ - x_2 (a_{H_2} + b_{H_2} x_{17}) - x_6 (a_{H_2O} + b_{H_2O} x_{17}) - h_a (x_{17} - x_{15}) + r_{sft} \Delta H_{sft} + [x_2 (a_{H_2} + b_{H_2} u_3) + h_a (u_3 - x_{15}) + x_6 (a_{H_2O} + b_{H_2O} x_{15}) - r_{sft} \Delta H_{sft}] . \exp \left(- \frac{1}{r^*} \frac{Rx_{17}}{u_2} \frac{x_2 b_{H_2} + h_a}{u_{fuel} \sum_{20}^{24} x_i b_i} \cdot z \right) \Big\}$$

$$\dot{x}_{18} = \frac{1}{r_2^*} \frac{1}{C_{p,air}} \frac{Rx_{18}}{u_5} \Big\{ - (h_c + \frac{r_1}{r_2} h_c) x_{18} - (-h_c x_{15} + \frac{r_1}{r_2} h_c x_{16}) + \left[(h_c + \frac{r_1}{r_2} h_c) x_{19}|_{x=0} + (-h_c x_{15} + \frac{r_1}{r_2} h_c x_{16}) \right] \cdot \left[1 - \frac{1}{2r_2^*} \frac{R}{u_5 \frac{r_0}{r_2 - r_1} u_7} x_4 (x_{19}|_{x=0} + x_{18}) \cdot z \right]^{-2 \frac{x_{18}}{x_{19}|_{x=0} + x_{18}}} \Big\}$$

$$\dot{x}_{19} = \frac{2}{r_0} \frac{1}{C_{p,air}} \frac{Rx_{19}}{u_5} \Big\{ - h_t x_{19} + h_t x_{16} + (h_t u_6 - h_t x_{16}) \exp \left[- \frac{2}{r_2} \frac{R}{u_5 u_7} \frac{h_t}{b_{air}} x_{19} \cdot (L - z) \right] \Big\}$$

$$\dot{x}_{20} = \frac{1}{z \cdot r^*} \frac{Rx_{17}}{u_2} \left\{ -u_{fuel} x_{20} + u_4 \chi_{CH_4}^{in} - r_{ref}^{in} \xi \left[1 - \exp \left(- \frac{z}{\xi} \right) \right] \right\}$$

$$\dot{x}_{21} = \frac{1}{z \cdot r^*} \frac{Rx_{17}}{u_2} \left\{ -u_{fuel} x_{21} + u_4 \chi_{H_2O}^{in} - r_{ref}^{in} \xi \left[1 - \exp \left(- \frac{z}{\xi} \right) \right] - (r_{sft} + x_6) \cdot z \right\}$$

$$\dot{x}_{22} = \frac{1}{z \cdot r^*} \frac{Rx_{17}}{u_2} \left\{ -u_{fuel} x_{22} + u_4 \chi_{H_2}^{in} + 3 r_{ref}^{in} \xi \left[1 - \exp \left(- \frac{z}{\xi} \right) \right] + (r_{sft} - x_2) \cdot z \right\}$$

$$\dot{x}_{23} = \frac{1}{z \cdot r^*} \frac{Rx_{17}}{u_2} \left\{ -u_{fuel} x_{23} + u_4 \chi_{CO}^{in} + r_{ref}^{in} \xi \left[1 - \exp(-\frac{z}{\xi}) \right] - r_{sft} \cdot z \right\}$$

$$\dot{x}_{24} = \frac{1}{z \cdot r^*} \frac{Rx_{17}}{u_2} \left\{ -u_{fuel} x_{24} + u_4 \chi_{CO_2}^{in} + r_{sft} \cdot z \right\}$$

$$\dot{x}_{25} = \frac{1}{r_2^*} \frac{Rx_{18}}{u_5} \Big\{ - (1 - x_{25}) x_4 + (1 - \chi_{O_2}^{in}) x_4 . \left[1 - \frac{1}{2r_2^*} \frac{R}{u_5 \frac{r_0}{r_2 - r_1} u_7} (x_{19}|_{z=0} + x_{18}) x_4 \cdot z \right]^{-2 \frac{x_{18}}{x_{19}|_{z=0} + x_{18}}} \Big\}$$

Outputs :

$$y_1 = \frac{1}{2} (x_1|_{z=0} + x_1|_{z=L}) - \rho_{R_o} l_{R_o} \frac{u_1}{2\pi r_3 L}$$

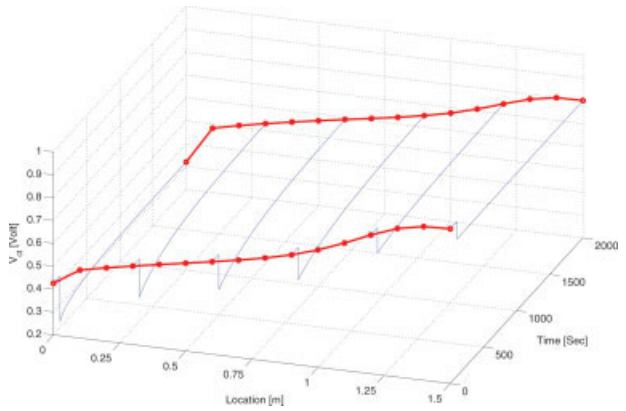

Figure 6. V_{ct} profile and step response, when I step changes from 100 to 150 Amp at 100 s.

[Color figure can be viewed in the online issue, which is available at www.interscience.wiley.com.]

$$y_2 = x_{17}|_{z=L}$$

$$y_3 = u_4 + 2\chi^{\text{in}}_{\text{CH}_4} u_4 \left[1 - \exp\left(-\frac{Rx_{17}|_{z=L}}{r^* u_2} \frac{r^{\text{in}}_{\text{ref}}}{u_4 \chi^{\text{in}}_{\text{CH}_4}} \cdot L\right)\right]$$

$$y_4 = x_{18}|_{z=L}$$

$$y_5 = \frac{r_0}{r_2 - r_1} u_7 - \frac{1}{2r_2^*} \frac{R}{u_5} (x_{19}|_{z=0} + x_{18}|_{z=L}) x_4|_{z=L} \cdot L$$

$$y_6 = x_{22}|_{z=L}$$

$$y_7 = x_{23}|_{z=L}$$

$$y_8 = x_{25}|_{z=L}$$

Where:

$$E = 1.273 - 2.7645 \times 10^{-4} x_{15} + \frac{Rx_{15}}{2F} \ln\left(\frac{x_8 x_{10}^{1/2}}{x_{12}}\right) - \frac{Rx_{15}}{F} \sinh^{-1}\left(\frac{\frac{u_1}{2\pi r_3 L}}{7 \times 10^9 (x_8 x_{12}) \exp(-\frac{E_{\text{act,a}}}{Rx_{15}})}\right) - \frac{Rx_{15}}{F} \sinh^{-1}\left(\frac{\frac{u_1}{2\pi r_3 L}}{7 \times 10^9 (x_{10})^{0.25} \exp(-\frac{E_{\text{act,c}}}{Rx_{15}})}\right)$$

$$u_{\text{fuel}} = u_4 + 2\chi^{\text{in}}_{\text{CH}_4} u_4 \left[1 - \exp\left(-\frac{Rx_{17}}{r^* u_2} \frac{r^{\text{in}}_{\text{ref}}}{u_4 \chi^{\text{in}}_{\text{CH}_4}} \cdot L\right)\right]$$

$$\xi = \frac{r^* u_2}{Rx_{17}} u_4 \chi^{\text{in}}_{\text{CH}_4}$$

$$r_{\text{ref}} = K_{\text{r}} (u_2 x_{20})^{\alpha} (u_2 x_{21})^{\beta} \exp\left(-\frac{E_{\text{r}}}{Rx_{17}}\right)$$

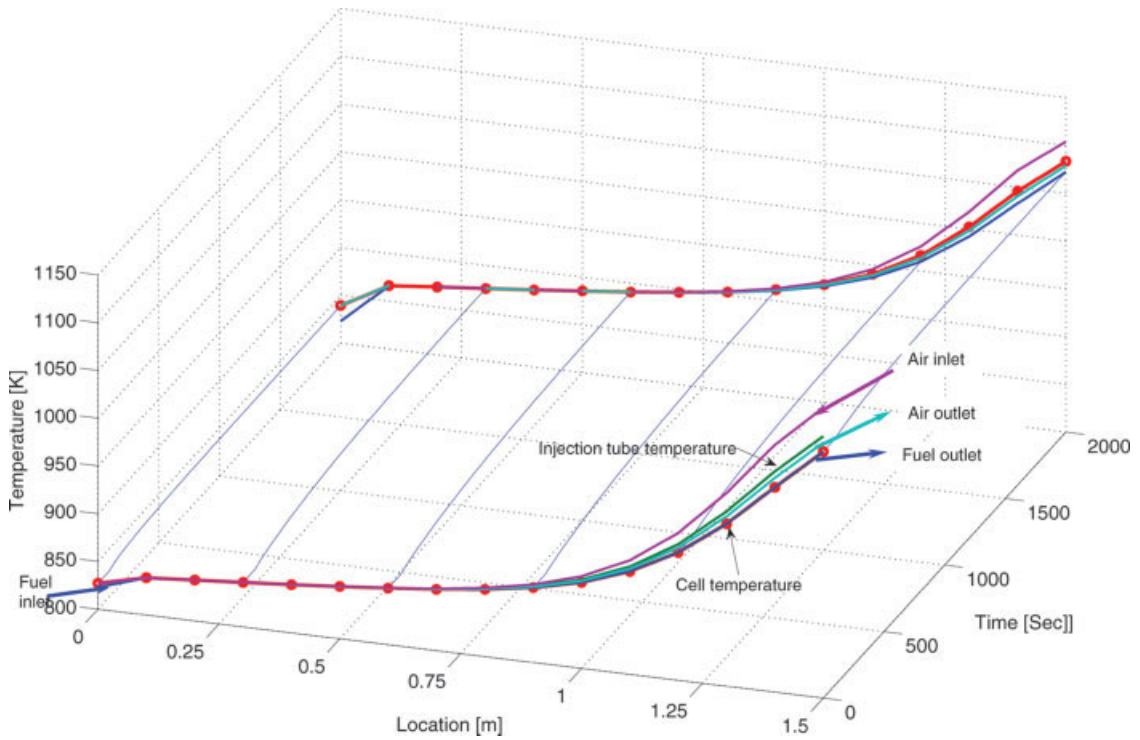

Figure 7. Profiles and step responses of temperatures, when I step changes from 100 to 150 Amp at 100 s.

[Color figure can be viewed in the online issue, which is available at www.interscience.wiley.com.]

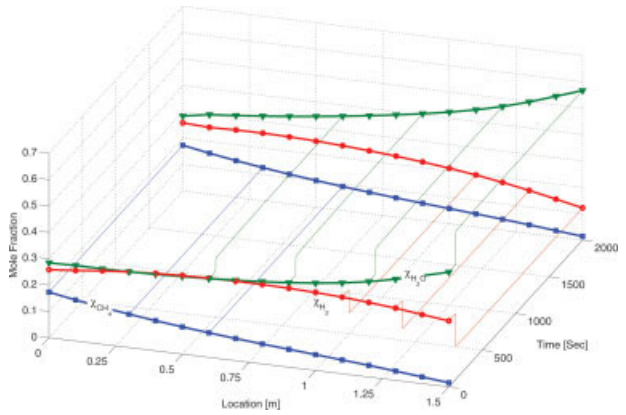

Figure 8. Profiles and step responses of species fractions, when *I* step changes from 100 to 150 Amp at 100 s.

[Color figure can be viewed in the online issue, which is available at www.interscience.wiley.com.]

$$r_{\text{ref}}^{\text{in}} = K_{\text{r}}(u_2\chi_{\text{CH}_4}^{\text{in}})^{\alpha}(u_2\chi_{\text{H}_2\text{O}}^{\text{in}})^{\beta}\exp\left(-\frac{E_{\text{r}}}{Ru_3}\right)$$

$$r_{\text{sft}} = K_{\text{s}}u_2^2\left[x_{23}x_{21}\exp\left(\frac{4276}{x_{17}}-3961\right)-x_{22}x_{24}\right]$$

or, in a compact form

$$\begin{aligned}\dot{\mathbf{x}} &= f(\mathbf{x},\mathbf{u},z)\\ \mathbf{y} &= g(\mathbf{x},\mathbf{u},z)\end{aligned} \tag{51}$$

Simulations

A Simulink model of the tubular SOFC with an analytical solution for the 1-D dynamic reacting gas-flow problem, has been developed according to the state-space equations. Dynamic behaviors and parameter distributions of SOFC were simulated through the model. The SOFC model parameters are listed in Table A2. Gas-phase parameters can be found in Qi et al.[11] Default input conditions for simulation are shown in Table A1. Perturbations of input variables are relative to these default settings.

Step responses due to current demand changes

Step response tests can effectively reveal process dynamic parameters, such as time constant, gain, time delay, etc. Step responses and distributed profiles of voltage, temperatures, and species mole fractions, etc., due to the step change in current demand *I* are shown in Figures. 6, 7, and 8, respectively.

When external load current demand *I* was stepped up, diffusion processes and the intrinsic impedance prevented the immediate jump of voltage, and the time constant of the consequent dynamic response is around 0.2 s.

Because more current was consumed by the inherent resistance, the cell, is, therefore, heated and its temperature is increased gradually as shown by Figure 7. The response time constant is around 500 s due to its large heat capacity and the turn-around-air-flow-route design. The behavior of cell temperature consequently dominates behavior of other temperatures.

Step change of current *I* changes the secondary reactant fluxes $j_{\text{H}_2}^{\text{s}}$, $j_{\text{H}_2\text{O}}^{\text{s}}$, and $j_{\text{O}_2}^{\text{s}}$. They consequently affect composition distributions, as shown by Figure 8. Obviously, their responses are dominated by the response of cell temperature.

Because air input rate is very high, the decrease of oxygen mole fraction due to the electrochemical reaction is minor. The profile is almost a flat line. So the cathode-side oxygen step response and profile are not shown in the figures.

Effect of fuel inlet

When fuel inlet pressure $P_{\text{fuel}}^{\text{in}}$ was stepped up, concentration of CH_4 increased immediately. So the reforming reaction rate increased. More H_2 was produced, and that changed the voltage response and composition distributions. The voltage V_{ct} then increased, and the step response is shown in Figure 9. Due to the faster reforming reaction, more heat was absorbed from the cell tube and its temperature dropped, shown in Figure 10.

When fuel inlet temperature $T_{\text{fuel}}^{\text{in}}$ was stepped up, the reforming reaction rate increased, and H_2 was produced faster. The voltage V_{ct} then increased as shown in Figure 11. Also, due to the temperature increase, the equilibrium of the shifting reaction moved, leading to significant composition profile change, as shown in Figure 12.

Step change of fuel inlet velocity $u_{\text{fuel}}^{\text{in}}$ changed the heat-transfer coefficient h_{a}. So heat was transferred from the cell to fuel. Therefore, it affected temperatures as shown in Figure 13. The change of velocity directly affected species distribution profiles.

Effect of air inlet

The step change of the air pressure affects the oxygen concentration, and then the voltage. Its effect on temperatures and compositions are, however, not so significant. The air inlet temperature step change affected the heating conditions of the SOFC from cathode side, and then the temperature profile as shown in Figure 14. Air inlet velocity also affected

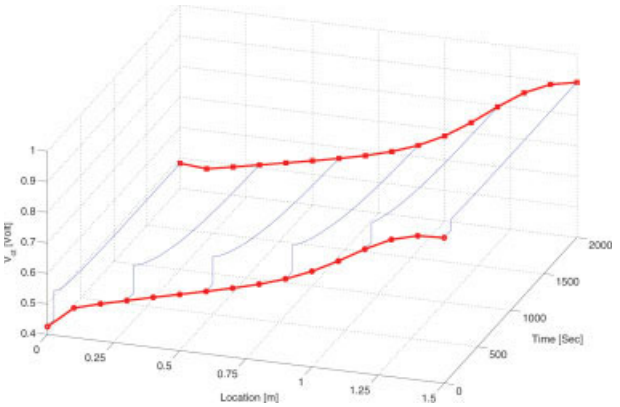

Figure 9. V_{ct} profile and step response, when $P_{\text{fuel}}^{\text{in}}$ step changes from 1 to 2 atm at 100 s.

[Color figure can be viewed in the online issue, which is available at www.interscience.wiley.com.]

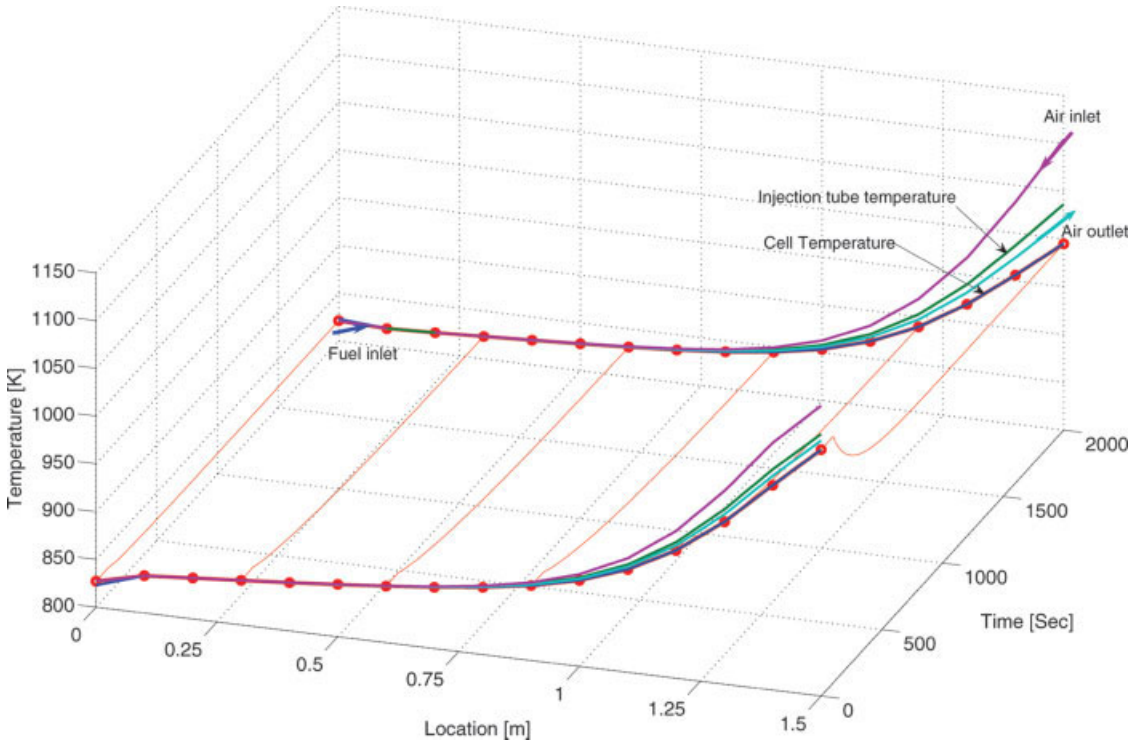

Figure 10. Profiles and step responses of temperatures, when P^{in}_{fuel} step changes from 1 to 2 atm at 100 s.

[Color figure can be viewed in the online issue, which is available at www.interscience.wiley.com.]

the temperature profile. However they did not directly affect the anode side parameters, and the effects were minor.

Conclusions

An 1-D dynamic model for a tubular solid oxide fuel cell (SOFC) stack has been developed. Distributed dynamic relations of current density and electromotive force (EMF) have been developed. Dynamics of solid-phases non flowing parameters has been investigated. Distributed dynamics of flowing phases, such as fuel-and airflow has been addressed by simultaneously considering diffusion, inherent impedance, primary flow, heat transfer, and internal reforming/shifting reactions. They are modeled in the form of partial differential equations (PDEs).

An approximated analytical solution for 1-D dynamic reacting gas-flow problem has been proposed. It has been applied to the 1-D SOFC model, and analytically solved velocity, mole fraction and temperature distributions for primary flows. PDEs in the 1-D dynamic model are then converted to ordinary differential equations (ODEs). Combined with the dynamic models for nonflowing parameters, the 1-D dynamic model for the tubular SOFC has been presented in the form of nonlinear state-space equations.

Dynamic performances and parameter distributions have been investigated through simulated step responses of the SOFC stack to changes of external current demand, and fuel and air input parameters, respectively. They are investigated along the whole length of the tube, and the results are presented.

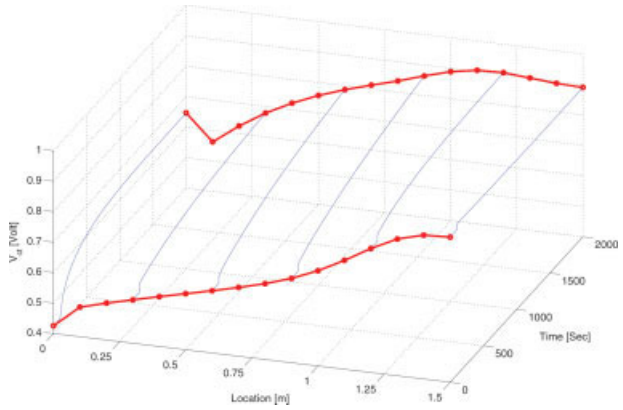

Figure 11. V_{ct} profile and step response, when T^{in}_{fuel} step changes from 823 to 923 K at 100 s.

[Color figure can be viewed in the online issue, which is available at www.interscience.wiley.com.]

Acknowledgments

This work is supported in part by WCFCI and NSERC.

Notation

C_{ct} = charge transfer capacity, F
C_p = specific heat at constant pressure, J mol^{-1} K^{-1}

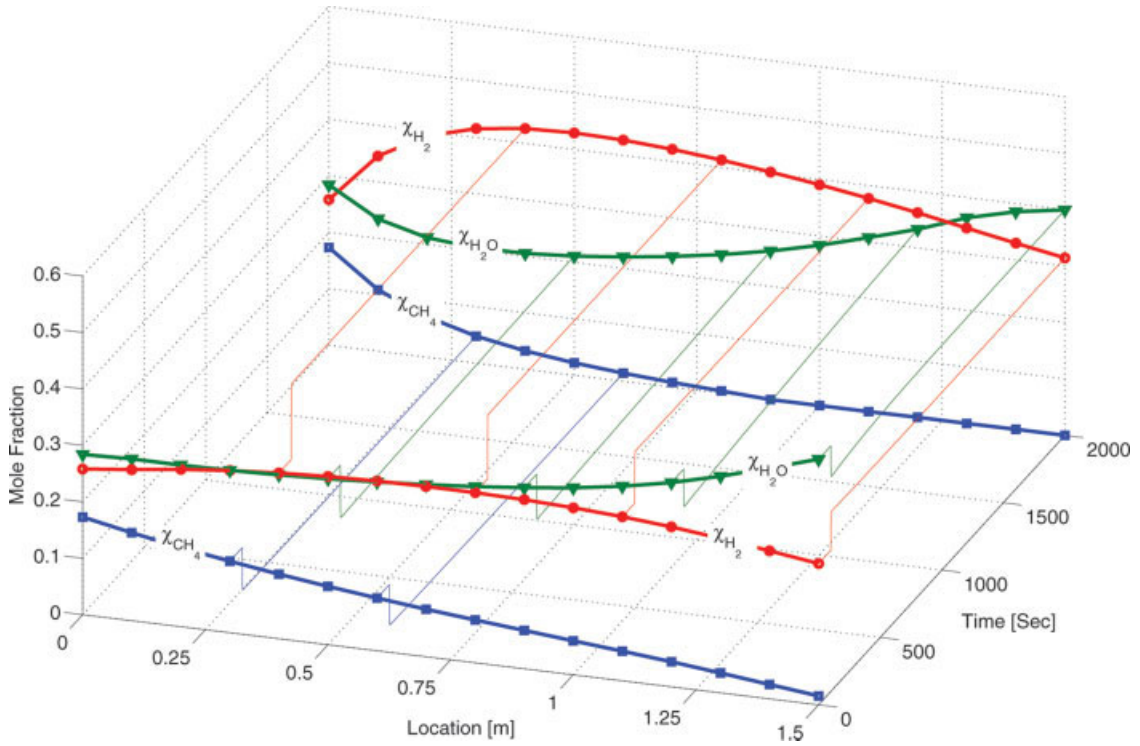

Figure 12. Profiles and step responses of species fractions, when T^{in}_{fuel} step changes from 823 to 923 K at 100 s.

[Color figure can be viewed in the online issue, which is available at www.interscience.wiley.com.]

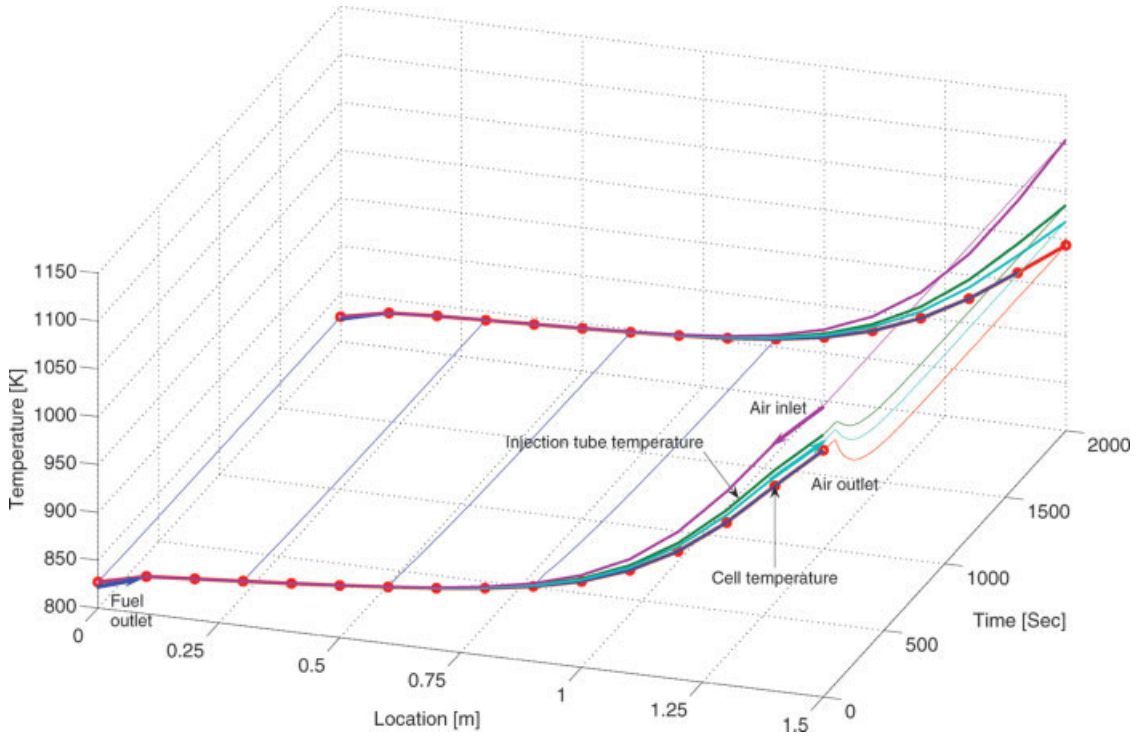

Figure 13. Profiles and step responses of temperatures, when u^{in}_{fuel} step changes from 0.927 to 1.927 m/s at 100 s.

[Color figure can be viewed in the online issue, which is available at www.interscience.wiley.com.]

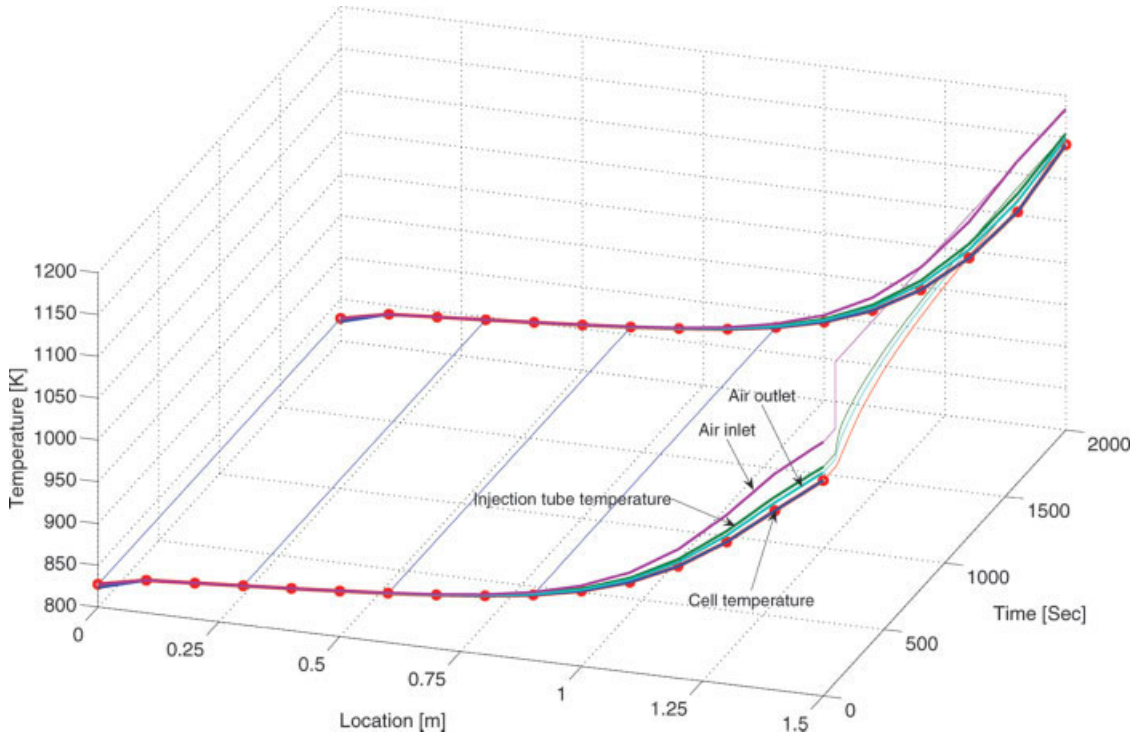

Figure 14. Profiles and step responses of temperatures, when T_{air}^{in} step changes from 1104 to 1184 K at 100 s.

[Color figure can be viewed in the online issue, which is available at www.interscience.wiley.com.]

D = diffusion coefficient, $m^2\ s^{-1}$
E = electromotive force, V
E_e = electrical power, J
E_r = activation energy of reforming reaction, J mol^{-1}
F = Faraday's constant, = 96487 C mol^{-1}
h = convection heat-transfer coefficient, W $m^2\ K^{-1}$
H = enthalpy of formation, J mol^{-1}
ΔH = reaction heat, J mol^{-1}
i = current density, A m^{-2}
j^s = mass flux flowing into the surface of cell, μmol $s^{-1}\ m^{-2}$
K = reaction rate coefficient
l = thickness, m
L = length of cell tube, m
M = mole mass, g mol^{-1}
p = partial pressure, atm
P = total pressure, atm
q = heat flux, J $s^{-1}\ m^{-2}$
r = radius of SOFC tube components, m
r_{ref} = reforming reaction rate, mol $s^{-1}\ m^{-2}$
r_{sft} = shifting reaction rate, mol $s^{-1}\ m^{-2}$
R = gas constant, = 82.05×10^{-5} J $mol^{-1}\ K^{-1}$
R_o = ohmic resistance, Ω
R_{ct} = charge transfer resistance, Ω
R_{rad} = radiation heat-transfer resistance
s = Laplace factor
T = temperature, K
u = flow velocity, m s^{-1}
V_{out} = fuel cell voltage out, V

Greek letters

μ = viscosity
ρ = density
ρ_{Rct} = specific resistance of charge transfer resistance $\Omega\ m^{-1}$
ρ_{Cct} = specific capacitance of charge transfer capacitance, $F\ m^2$
ρ_{Ro} = specific resistance of pure Ohmic resistance, $\Omega\ m^{-1}$
σ = Stefan-Boltzmann constant, = 5.6697×10^{-8} W $m^{-2}\ K^{-4}$
χ = mole fraction
ξ = space constant

Superscripts

in = inlet
out = outlet

Subscripts

0 = inner surface of injection tube
1 = outer surface of injection tube
2 = inner surface of cell tube
3 = outer surface of cell tube
a = anode side
c = cathode side
cell = cell tube
conv = convection
cond = conduction
eq = equilibrium
f = fluid
i = fuel ingredients
j = air ingredients
rad = radiation
ref = reforming reaction
sft = shifting reaction
t = inside injection tube
w = wall

Literature Cited

1. Achenbach E. Three-dimensional and time dependent simulation of a planar solid oxide fuel cell stack. *J of Power Sources*. 1994;49:333–348.

2. Achenbach E. Response of a solid oxide fuel cell to load change. *J of Power Sources*. 1995;57:105–109.
3. Padullés J, Ault GW, McDonald JR. An integrated SOFC plant dynamic model for power systems simulation. *J of Power Sources*. 2000;86:495–500.
4. Zhu Y, Tomsovic K. Development of models for analyzing the load-following performance of microturbines and fuel cells. *Electric Power Systems Res*. 2001;62:1–11.
5. Sedghisigarchi K, Feliachi A. Dynamic and transient analysis of power distribution systems with fuel cells-part I. *IEEE Trans on Energy Conversion*. 2004;19:423–428.
6. Li Pei-Wen, Chyu Minking K. Simulation of the chemical/electrochemical reactions and heat/mass transfer for a tubular SOFC in a stack. *J of Power Sources*. 2003;124:487–498.
7. Xue X, Tang J, Sammes N, Du Y. Dynamic modeling of single tubular SOFC combining heat/mass transfer and electrochemical reaction effects. *J of Power Sources*. 2005;142:211–222.
8. Gemmen RS, Johnson CD. Effect of load transients on SOFC operation — current reversal on loss of load. *J of Power Sources*. 2005;144:152–164.
9. Iora P, Aguiar P, Adjiman CS, Brandon NP. Comparison of two IT DIR-SOFC models: Impact of variable thermodynamic, physical and How properties. Steady-state and dynamic analysis. *Chem Eng Sci*. 2005;60:2963–2975.
10. Qi Y, Huang B, Chuang KT. Dynamic modeling of solid oxide fuel cell: The effect of diffusion and inherent impedance. *J of Power Sources*. 2005;150:32–47.
11. Qi Y, Huang B, Luo J. Dynamic modeling of a finite volume of solid oxide fuel cell: The effect of transport dynamics. *Chem Eng Sci*. 2006;61:6057–6076.
12. Ahmed Khaliq, Foger Karl. Kinetics of internal steam reforming of methane on Ni/YSZ-based anodes for solid oxide fuel cells. *Catalysis Today*. 2000;63:479–487.
13. Murshed AKM M, Huang B, Nandakumar K. Control relevant modeling of planar solid oxide fuel cell system. *J of Power Sources*. 2007;163:830–845.
14. Zucker RD, Biblarz Oscar. *Fundamentals of Gas Dynamics*. 2 ed.; John Wiley and Sons, Inc. 2002.
15. Campanari S, Iora P. Definition and sensitivity analysis of a finite volume SOFC model for a tubular cell geometry. *J of Power Sources*. 2004;132:113–126.
16. Perry RH, Green DW, Maloney JO. eds. *Perry's Chemical Engineers' Handbook*. 7th ed.; New York, London, Mexico City, Milan, Montreal, New Delhi, Singapore, Sydney, Tokyo, Toronto: McGraw-Hill, Inc. 1997.
17. Hall DJ. Transient Modeling and Simulation of a Solid Oxide Fuel Cell. University of Pittsburgh; 1997. PhD thesis.
18. Bessette NF. Modeling and Simulation for Solid Oxide fuel Cell Power Systems. Georgia Institute of Technology; 1994. PhD thesis.

Appendix

Input conditions of simulation are shown in Table A1. Other parameters of SOFC are shown in Table A2.

Table A1. Simulation Input Conditions

Symbol	Description	Source
$I = 200$ Amp	External load current demand	
$P^{in}_{fuel} = 1$ atm	Fuel inlet pressure	15
$T^{in}_{fuel} = 823$ K	Fuel inlet temperature	15
$u^{in}_{fuel} = 0.927$ m/s	Fuel inlet velocity	15
$P^{in}_{air} = 1$atm	Air inlet pressure	15
$T^{in}_{air} = 1104$ K	Air inlet temperature	15
$u^{in}_{air} = 12.08$ m/s	Air inlet velocity	15
$\chi^{in}_{CH_4} = 0.173$	Inlet mole fraction of CH_4	15
$\chi^{in}_{H_2O} = 0.284$	Inlet mole fraction of H_2O	15
$\chi^{in}_{H_2O} = 0.258$	Inlet mole fraction of H_2	15
$\chi^{in}_{CO} = 0.057$	Inlet mole fraction of CO	15
$\chi^{in}_{CO_2} = 0.228$	Inlet mole fraction of CO_2	15
$\chi^{in}_{O_2} = 0.21$	Inlet mole fraction of O_2	

Table A2. Model Parameters

Symbol	Description	Source	Symbol	Description	Source
Geometry parameters					
$r_3 = 11 \times 10^{-3}$ m	Radius of outer cell tube	15	$\rho_c = 8.11 \times 10^{-5} \cdot \exp\left(\frac{600}{T_{cell}}\right)$ Ωm	Specific resistivity of cathode	18
$r_2 = 8.66 \times 10^{-3}$ m	Radius of inner cell tube	15			
$r_1 = 6 \times 10^{-3}$ m	Radius of outer Injection tube	15	$\rho_{tube} = 3900$ kg/m^3	Density of injection tube	17
$r_0 = 5 \times 10^{-3}$ m	Radius of inner injection tube	15	$C_{p,tube} = 976.8 + 0.2409T$ J/(kgK)	Specific heat of injection tube	17
$l_a = 0.1 \times 10^{-3}$ m	Thickness of anode	15	$k_{tube} = 31.86 - 0.03706T + 1.317 \times 10^{-5}T^2$ W/(mK)	Conductivity of injection tube	17
$l_c = 2.21 \times 10^{-3}$ m	Thickness of cathode	15	$\varepsilon_{cell} = 0.4$	Emissivity of cell inner surface	17
$l_e = 0.04 \times 10^{-3}$ m	Thickness of electrolyte	15			
$F_{c\text{-}t} = 0.69$	View factor: cell to injection tube	16	*Reforming and shifting*		
Properties of solid materials			$K_r = 8542$	Reforming reaction rate coefficient	12
$\rho_{cell} = 4592$ kg/m^3	Entire density of SOFC cell	17	$K_s = 100$	Shift reaction rate coefficient	
$C_{p,cell} = 740$ J/(kgK)	Entire specific heat of SOFC cell	17	$E_r = 95$ KJ/mol	Activation of reforming reaction	12
$k_{cell} = 2.0$ W/(mK)	Entire conductivity of anode	15	$\alpha = 0.85$	order coefficient of reforming	12
$\varepsilon_{cell} = 0.9$	Emissivity of cell inner surface	17	$\beta = -0.35$	order coefficient of reforming	12
$\rho_a = 2.98 \times 10^{-5} \cdot \exp(-\frac{1392}{T_{cell}})$ Ωm	Specific resistivity of anode	18			
$\rho_e = 2.94 \times 10^{-5} \cdot \exp(\frac{10350}{T_{cell}})$ Ωm	Specific resistivity of electrolyte	18			

Manuscript received May 20, 2007, and revision received Dec. 9, 2007.